Available online at www.sciencedirect.com
SCIENCE DIRECT®
Journal of Catalysis 225 (2004) 24–36
JOURNAL OF CATALYSIS
www.elsevier.com/locate/jcat

# Vanadia–silica and vanadia–cesium–silica catalysts for oxidation of $SO_2$

Vasile I. Pârvulescu,[a,*] Cristina Paun,[a] Viorica Pârvulescu,[a] Mihai Alifanti,[a] Ioanna Giakoumelou,[b] Soghomon Boghosian,[b,*] Soren B. Rasmussen,[c] Kim M. Eriksen,[c] and Rasmus Fehrmann[c,*]

[a] *University of Bucharest, Department of Chemical Technology and Catalysis, B-dul Regina Elisabeta 4-12, Bucharest 70346, Romania*
[b] *Department of Chemical Engineering, University of Patras and Institute of Chemical Engineering and High Temperature Chemical Processes (FORTH/ICE-HT), GR-26500, Patras, Greece*
[c] *Interdisciplinary Research Center for Catalysis (ICAT), Department of Chemistry, Tehnical University of Denmark, DK-2800 Lyngby, Denmark*

Received 9 December 2003; revised 24 March 2004; accepted 31 March 2004

Available online 24 April 2004

**Abstract**

Mesoporous vanadia–silica catalysts have been prepared by three different sol–gel procedures using tetraethylorthosilicate (TEOS), vanadyl acetylacetonate (VAA), or $VOCl_3$ and in some cases quaternary ammonium salts ($(CH_3)_3C_{14}H_{29}N^+Br^-$ or $(C_{10}H_{21})_4N^+Br^-$) as surfactants. According to procedure A, TEOS and VAA were concomitantly hydrolyzed, in procedure B TEOS was prehydrolized and vanadium precursor was added to the silica sol, and in procedure C both TEOS and vanadium precursors were separately prehydrolized. The sol–gel procedures were controlled by checking the effect of the hydrolysis pH, refluxing time, surfactant, and conditions of gellifications (slow evaporation at room temperature or autoclavization). The samples were dried under vacuum, first at room temperature, then at 373 K, and finally calcined at 773 K. ICP-AES analysis indicated for all samples a vanadium content of around 6.5 wt%. The samples were impregnated with $Cs_2SO_4$ resulting in a Cs:V ratio of 3:1 and then dried and calcined under the same conditions. The catalysts were characterized using several methods: sorption isotherms of $N_2$ at 77 K, XRD, and XPS. The results of the characterization indicated that during calcination of the V/Cs catalysts vanadia is dissolved in a sulfate containing molten salt. The activity of these catalysts for the oxidation of $SO_2$ was tested in a gas containing 2% $SO_2$, 19% $O_2$, 79% $N_2$ in the temperature range 523–823 K. Similar experiments with gases containing 10% $H_2O$ in the feed or with wet catalysts were also performed. The activation of the catalysts and the catalytic behavior were monitored by in situ Raman and EPR spectroscopy. These characterization techniques indicated that the active molten phase contains vanadium oxosulfato complexes similar to the $V_2O_5$–$M_2S_2O_7$ ($M$ = alkali metal)-based industrial catalyst, where kieselghur is used as carrier material. The high dispersion of vanadium in the studied catalysts results in an increased catalytic activity for the oxidation of $SO_2$ contained in feed gases with low $SO_2$ content.


*Keywords:* Mesoporous $V_2O_5$–$SiO_2$ catalysts promoted with Cs; In situ Raman; EPR; XRD characterization

## 1. Introduction

Sulfur dioxide emitted both from industrial processes (primarily sulfuric acid manufacture, petroleum refining, and smelting of nonferrous metals) and by the oxidation of sulfur contained in fossil fuels is responsible for acid rain and its abatement is a major environmental problem [1]. Technologies generally used for abatement of $SO_2$ include the limestone process [2], the selective adsorption of $SO_2$ on, e.g., promoted alumina [3,4], and the Claus process [5], which, however, all generate considerable amounts of by-products. The use a $SO_x$-reduction catalyst using supported vanadia catalysts, such as the Amoco De$SO_x$ catalyst ($V_2O_5/CeO_2/Mg_2Al_2O_5$) may lead to better recovery of sulfur [6].

The catalytic alternatives, however, may provide promising clean environmental solutions. Some of these technologies dealing with the simultaneous removal of $SO_x$ and $NO_x$ from flue gas are already industrially applied. Among these, the well-known Haldor Topsøe SNOX [7] and Degussa De$SONO_x$ [8] processes combine the selective catalytic reduction (SCR) of $NO_x$ with production of sulfuric

* Corresponding authors.
*E-mail addresses:* v_parvulescu@chem.unibuc.ro (V.I. Pârvulescu), bogosian@iceht.forth.gr (S. Boghosian), rf@kemi.dtu.dk (R. Fehrmann).

0021-9517/$ – see front matter 
doi:10.1016/j.jcat.2004.03.040

acid. First, $NO_x$ gases are removed via the SCR technology and then $SO_2$ is oxidized to $SO_3$ over a typical oxidation catalyst.

The oxidation of $SO_2$ to $SO_3$ resulting in sulfuric acid manufacture is an attractive approach. Most of the flue gases from metallurgical plants contain $SO_2$. The main difficulty for achieving high conversions is the low $SO_2$ content in these gases ($< 3\%$). This is critical since the reactor in the contact process operates in autothermal regime, so the amount of heat generated depends on the $SO_2$ content in the feed. In the case of dilute gases the evolved heat is not enough to allow for satisfactory reaction rates. Improvements in the reactor design, as the nonstationary reactor with flow reversal [9,10] may lead to higher efficiency of this reaction for gases with low $SO_2$ contents.

However, an important contribution for improvement of direct $SO_2$ oxidation of dilute gases could come from the development of new catalysts, specifically tailored for this purpose. Actually, the industrial catalyst is a unique supported liquid-phase catalyst (vanadium oxides with alkali promoters forming a pyrosulfate melt supported on kieselghur). Under reaction conditions, 693–823 K, the $SO_2$ oxidation proceeds on active sites located in the interior of the liquid film and recently, the V(V) dimeric complex $(VO)_2O(SO_4)_4^{4-}$ has been identified as the catalytically active species [11–17]. Detailed investigations of the effect of the promoters (Na, K, Cs) showed that the activity increases with increasing alkali atomic number, and the presence of Cs as a promoter improves the low-temperature activity with the deactivation occurring at temperatures below 673 K [18–21].

A possible way to enhance the efficiency of these catalysts making them able to oxidize gases very dilute in $SO_2$ is to increase the surface area, while keeping the size of the pores in a comparable range with that of silica used in industrial applications. Such characteristics can be provided by mesoporous catalysts, in which vanadia is directly introduced during synthesis. The preparation of catalysts containing highly dispersed vanadium has thus received much interest. Over the years, several preparation procedures have been proposed like impregnation of inorganic supports using various salts in both aqueous (silica, titania, diathomite) [22] and nonaqueous procedures [22–24], dry impregnation using vanadium pentoxide as precursor [25–28], incorporation of vanadia using hydrothermal procedures [29–31], vapor-phase grafting of $VOCl_3$ on silica [32–35], and sol–gel procedures. The use of sol–gel procedures received particular interest because of the characteristics reported for the materials obtained by this route. Due to large differences in the reaction rates between the metal alcoxides and the silicon alcoxides it is generally considered as being difficult to achieve homogeneity in mixed metal oxides using this technique [36]. However, studies made by Baiker and co-workers. [37,38] showed the effectivity of polymeric sol–gel procedures to produce very homogeneous mixed oxides leading to high dispersion of vanadium, combined with high surface areas, narrow pore size distribution, and high stability. To achieve isolated vanadyl species, Rulkens et al. [39] proposed an alternative route using a different source of vanadium, i.e., vanadyl *tert*-butoxyorthosilicate. Livage and co-workers reported colloidal sol–gel preparations and showed that depending on pH and concentration, the vanadium species can condense leading to polymeric species [40]. V-MCM-41-type materials have also been prepared [41] containing tetrahedrally coordinated vanadium, which may suggest insertion of vanadium in the silica framework. These preparations evidenced the effect of the surfactant on both the stability and the pore size. However, V-MCM-41 is not sufficiently stable at high temperatures and in the presence of water.

The state of vanadium in these materials is evidently connected with the preparation procedure. Low vanadium loading leads to highly dispersed, e.g., monomeric or oligomeric species where vanadium appears isolated and tetracoordinated under dehydrated conditions. The increase of loading results in formation of polymeric two-dimensional species in distorted tetrahedral and square-pyramidal coordination, and bulk $V_2O_5$ crystals are formed when vanadia loading exceeds the monolayer coverage of the support. The addition of alkaline metal sulfates to vanadia catalysts leads, at higher temperatures, to molten salt mixtures, which exhibit low melting points [11,13,42,43].

The aim of the present study is to investigate the preparation of high surface area disordered silica–vanadia catalysts with sol–gel procedures. The variations caused in the textural characteristics by the preparation routes used are presented. The catalysts are investigated for $SO_2$ oxidation in feed gases with low $SO_2$ content, i.e., less than 2%. The effect of $Cs_2SO_4$ addition both on textural and on structural characteristics of these catalysts as well as its promoting effect on the activity is studied by combined catalytic tests and in situ Raman and EPR spectroscopy.

## 2. Experimental

### 2.1. Catalysts preparation

#### 2.1.1. Reagents

The reagents were tetraethylorthosilicate (TEOS, Aldrich, $> 99\%$ purity), vanadylacetylacetonate (VAA, Aldrich), vanadyloxychloride (Aldrich), trimethyltetradecylammonium bromide (Merck), tetradecylammonium bromide HCl (Merck), ammonium hydroxide (Merck), methanol (Merck), and $Cs_2SO_4$ (Merck).

#### 2.1.2. Sol–gel synthesis

The synthesis of the catalysts was carried out following three routes.

*2.1.2.1. Method (a).* VAA was dissolved in methanol with a molar ratio VAA-to-methanol of 0.013. TEOS was added dropwise to this solution, maintaining the system under

vigorous stirring. The amount of TEOS added was calculated for molar TEOS-to-VAA ratio of 11.54 and TEOS-to-methanol ratio of 0.15. The pH of the solutions was different. For samples prepared under acid catalysis, pH was adjusted to 3 with HCl, before the addition of water (a water-to-TEOS ratio of 4) (samples A1–A9), while for samples prepared under basic catalysis, the pH was adjusted to 9 with an aqueous solution of $NH_3$ after the addition of water (a water-to-TEOS ratio of 4) (samples A10–A12). The mixture was then refluxed at 338 K under vigorous stirring for various periods: 1 h (samples A1, A6, A8, and A10), 3 h (A2, A4, and A7), or 5 h (A3, A5, A9, A11, and A12). Thereafter the mixture was cooled at room temperature still under vigorous stirring and refluxing. Part of these samples was mixed with a methanol solution of a quaternary salt, which was prepared by dissolution of 1 g of $(CH_3)_3C_{14}H_{29}N^+Br^-$ (A1–A3, A5, and A8–A11) or 2 g of $(C_{10}H_{21})_4\,N^+Br^-$ (A4) in 2 ml methanol. The stirring was continued for 40 min for these mixtures. The sol polymerization and the aging of the gels were carried out either at 373 K for 5 days in a Teflon autoclave (A1–A7, A10–A12, B13–B19, and C20–C23) or by slow evaporation of the solvent at room temperature for one week (A8 and A9).

*2.1.2.2. Method (b).* TEOS was dissolved in methanol with a molar ratio TEOS-to-methanol of 0.5 under vigorous stirring. The pH of the solution was then adjusted to 3 with HCl (samples B13–B15) or to 9 with a solution of $NH_3$ (B16–B19). The addition of water was made considering the precautions presented in (a). The system was refluxed at 353 K for 30 min under vigorous stirring. VAA (B14, B16, and B18) or $VOCl_3$ (B13, B15, B17, and B19) was added as solutions in methanol (V-to-methanol molar ratio of 0.02) after the mixture was cooled at room temperature under the same stirring conditions; 1 g ammonium quaternary salt ($(CH_3)_3C_{14}H_{29}N^+Br^-$ in 2 ml methanol) was added after 40 min vigorous stirring and the mixture was then stirred for another 40 min (B13, B14, B16, and B19). The sol polymerization and the aging of the gels were carried out las in (a), namely at 373 K for 5 days in a Teflon autoclave (B13–B18) or by slow evaporation of the solvent at room temperature for 1 week (B19).

*2.1.2.3. Method (c).* TEOS was dissolved in methanol with a molar ratio TEOS-to-methanol of 0.5 under vigorous stirring. pH was adjusted to 3 with HCl. Water for prehydrolysis was then added with a molar ratio water-to-TEOS of 2 and the mixture was refluxed at 353 K for 30 min under vigorous stirring. Separately, VAA (C21–C23) or $VOCl_3$ (C20) was dissolved in methanol with a molar ratio V-to-methanol of 0.2 and the pH was modified with HCl to 3. Then, water for prehydrolysis was added to a molar ratio V-to-water of 0.043 (C20–C22). Sample C23 was obtained under basic hydrolysis where the addition of water to the VAA solution was made in the same ratio but before the adjustment of pH to 9. In both cases the mixture was then refluxed for 1 h at 338 K under vigorous stirring. After cooling, the prehydrolyzed vanadium was added to prehydrolyzed TEOS and the refluxing was continued for another 2 h at 338 K, under vigorous stirring. After cooling, 1 g of $(CH_3)_3C_{14}H_{29}N^+Br^-$ in 2 ml methanol was added to the above mixtures and stirred 40 min more (C20 and C21–C22). The sol polymerization and the aging of the gels were carried out as in (a), namely at 373 K for 5 days (C20–C21 and C23) or by slow evaporation of the solvent at room temperature for 1 week (C22). All samples were dried in vacuo, first at room temperature for 24 h, then at 373 K for another 24 h, and finally calcined at 773 K using a ramp of 0.3 K $min^{-1}$. ICP-AES analysis indicated for all samples a vanadium content of $\sim 6.5$ wt%.

These catalysts (denoted as Ax, Bx, and Cx) were promoted with Cs by incipient wetness impregnation using $Cs_2SO_4$, leading to catalysts with a Cs:V molar ratio of 3:1. The Cs-promoted samples are denoted as AxCs, BxCs, and CxCs, respectively.

### 2.2. Catalysts characterization

#### 2.2.1. Texture measurements

Sorption isotherms of $N_2$ at 77 K were obtained with a Micromeritics ASAP 2000 apparatus after outgassing the samples at 423 K for 12 h in vacuo. For the samples containing cesium, which exhibit low surface areas, the sorption isotherms were obtained with the same apparatus and temperature using Kr.

#### 2.2.2. X-ray diffraction

The XRD patterns were recorded by a SIEMENS D-5000 diffractometer at 40 kV, 50 mA, and equipped with a variable-slit diffracted-beam monochromator and scintillation counter. The diffractograms were recorded in the range 0–80° $2\theta$ $min^{-1}$ using Cu-$K_\alpha$ radiation ($\lambda = 1.54183$ Å).

#### 2.2.3. X-ray photoelectron spectroscopy

The XPS spectra were obtained by a SSI X probe FISONS spectrometer (SSX-100/206) with monochromated Al-$K_\alpha$ radiation. The spectrometer energy scale was calibrated using the Au $4f_{7/2}$ peak (binding energy 84.0 eV). For the calculation of the binding energies, the $C_{1s}$ peak of the C–(C,H) component at 284.8 eV was used as an internal standard. The composite peaks were decomposed by a fitting routine included in the ESCA 8,3 D software. The superficial composition of the investigated samples was determined using the same software. The $V_{2p3}$, $Si_{2p}$, $Cs_{3d5}$, $Cs_{3d3}$, and $O_{1s}$ peaks were investigated.

### 2.3. Catalytic activity

Activity measurements were performed in a fixed-bed quartz microreactor operating at atmospheric pressure. Catalyst samples of 20–30 mg were used. The total flow rate was 100 ml $min^{-1}$ and the feed gas composition was 2% $SO_2$,

19% $O_2$, and 79% $N_2$. The catalytic tests were typically conducted in the temperature range 623–823 K, and in dry gas. Experiments with gases containing 10% $H_2O$ in the feed or with wet catalysts were also made. The inlet and outlet gas compositions were measured using an on-line coupled Fisher–Rousemount analyzer equipped with a UV detector.

### 2.4. In situ characterization

In situ Raman spectra were obtained using ∼ 150 mg of the catalysts, which were pressed into self-supporting wafers and mounted on an adjustable holder in the center of the in situ Raman furnace, which is a kanthal-wound double-wall quartz tube furnace mounted on a xyz plate. Temperature was controlled with a thermocouple placed inside the holder, near the catalyst. The gases used were $O_2$ (L'Air Liquide 99.995%), $SO_2$ (Matheson, Union Carbide 99.98% anhydrous), and $N_2$ (L'Air Liquide 99.999%) as a balance gas and were mixed by using thermal mass flowmeters (Brooks 5850E). The gas feed consisted of 0.4% $SO_2$ and 4% $O_2$ balanced in $N_2$ at a total flow rate of 50 ml $min^{-1}$.

In situ Raman spectra were recorded using the 488.0 nm line of an $Ar^+$ ion laser (Spectra Physics Model 164) at a power level of 30 mW, focused on the catalytic wafer by a cylindrical lens in order to reduce sample irradiance. The scattered light was collected at 90° (horizontal scattering plane), analyzed with a 0.85 m Spex 1403 double monochromator, and detected by a 253 K cooled RCA photomultiplier equipped with EG&G photon counting electronics. Each sample was oxidized at 673–773 K under $O_2$ flow for more than 2 h, and the in situ spectrum of the oxidized catalyst was recorded under flowing $O_2$. The catalyst was then exposed to the reaction mixture ($SO_2/O_2/N_2$) and spectra were recorded at different temperatures in the range 573–773 K.

EPR spectra were recorded on a Bruker EMX spectrometer equipped with a 12 kW 10 inch magnet. The spectra were acquired in situ with a high-temperature X-band Bruker ER4114HT cavity. This was done by using a Wilmad quartz high-temperature sample holder modified into a catalytic microreactor, allowing for simultaneous measurements of catalytic activity and EPR spectra of the working catalyst. The microwave frequency was around 9.53 GHz, and a scan range of 2000 Gauss was used for all recorded spectra, with a center field of 3500 Gauss. Acquisition was performed at least 20 min after thermal equilibrium was attained.

## 3. Results and discussion

### 3.1. Textural characteristics

The textural characteristics of the investigated catalysts are compiled in Table 1. These data reveal the effect of the preparation procedure on the textural characteristics, where the effect of hydrolysis and prehydrolysis seems most important.

Table 1
Preparative conditions, surface area, and pore-size diameter for the investigated samples

| Catalyst | Hydrolysis pH | Vanadium precursor | Surfactant | Gellation[a] | Without $Cs_2SO_4$ deposition | | After $Cs_2SO_4$ deposition | |
|---|---|---|---|---|---|---|---|---|
| | | | | | Surface area ($m^2\,g^{-1}$) | Mean pore size (nm) | Surface area ($m^2\,g^{-1}$) | Mean pore size (nm) |
| A1 | Acidic | VAA | $(CH_3)_3C_{14}$ | AUT | 489 | 1.8 | 5 | |
| A2 | Acidic | VAA | $(CH_3)_3C_{14}$ | AUT | 611 | 3.3 | 6 | 59.0 |
| A3 | Acidic | VAA | $(CH_3)_3C_{14}$ | AUT | 594 | 3.5 | 6 | 29.0 |
| A4 | Acidic | VAA | $(C_{10}H_{21})_4$ | AUT | 626 | 3.3 | 19 | 35.0 |
| A5 | Acidic | VAA | $(CH_3)_3C_{14}$ | AUT | 529 | 3.7 | 5 | |
| A6 | Acidic | VAA | None | AUT | 463 | 3.5 + 11.0 | 29 | 43.0 |
| A7 | Acidic | VAA | None | AUT | 753 | 4.0 + 12.0 | 9 | 54.0 |
| A8 | Acidic | VAA | $(CH_3)_3C_{14}$ | EVAP | 789 | 3.5 | 19 | 34.0 |
| A9 | Acidic | VAA | $(CH_3)_3C_{14}$ | EVAP | 777 | 4.5 | 21 | 23.0 |
| A10 | Basic | VAA | $(CH_3)_3C_{14}$ | AUT | 448 | 21.0 | 67 | 14.0 |
| A11 | Basic | VAA | $(CH_3)_3C_{14}$ | AUT | 97 | 42.0 | 9 | 48.0 |
| A12 | Basic | VAA | None | AUT | 16 | 48.0 | 4 | |
| B13 | Acidic | $VOCl_3$ | $(CH_3)_3C_{14}$ | AUT | 669 | 2.5 | 26 | 16.0 |
| B14 | Acidic | $VOCl_3$ | $(CH_3)_3C_{14}$ | AUT | 536 | 3.7 | 5 | |
| B15 | Acidic | $VOCl_3$ | None | AUT | 544 | 3.5 + 14.0 | 14 | 39.0 |
| B16 | Basic | VAA | $(CH_3)_3C_{14}$ | AUT | 373 | 11.0 | 25 | 19.0 |
| B17 | Basic | $VOCl_3$ | None | AUT | 248 | 3.5 + 28.0 | 7 | |
| B18 | Basic | VAA | None | AUT | 331 | 10.0 + 38.0 | 41 | 14.0 |
| B19 | Basic | $VOCl_3$ | $(CH_3)_3C_{14}$ | EVAP | 825 | 3.8 | 18 | 45.0 |
| C20 | Acidic | $VOCl_3$ | $(CH_3)_3C_{14}$ | AUT | 551 | 3.6 | 14 | 410 |
| C21 | Acidic | VAA | $(CH_3)_3C_{14}$ | AUT | 533 | 3.6 | 11 | 50.0 |
| C22 | Acidic | VAA | $(CH_3)_3C_{14}$ | EVAP | 828 | 3.7 | 9 | |
| C23 | Acidic | VAA | None | AUT | 708 | 4.0 | 35 | 28.0 |

[a] AUT, autoclavization; EVAP, evaporation.

*3.1.1. Hydrolysis under low pH*

The samples prepared under acidic hydrolysis had surface areas higher than around 500 $m^2\,g^{-1}$ and pore sizes in the range 1.8–4.5 nm (Table 1). Differences among these samples result from the effect of prehydrolysis, refluxing time, and the use of surfactant.

The increase of the refluxing time had a different effect on the surface area and pore size (Table 1, see A1–A3, A4–A5, A8–A9). The surface area reached a maximum after 3 h refluxing time, while the pore size continuously increased till 5 h. The adsorption–desorption isotherms of nitrogen at 77 K correspond to mesoporous materials, and the pore-size distribution is rather narrow, indicating a monomodal distribution, which results from the presence of the surfactant. Absence of the surfactant results in slightly larger pores and bimodal pore-size distribution (see A6, A7 in Table 1). On the other hand, the surfactant type, namely $(CH_3)_3C_{14}H_{29}N^+Br^-$ or $(C_{10}H_{21})_4\,N^+Br^-$ did not have an important influence on surface areas and pore sizes (Table 1, see A2 and A4).

*3.1.2. Hydrolysis at high pH*

The textural properties of the catalysts prepared under basic hydrolysis are different than those of the samples prepared under acidic hydrolysis. However, the same factors were found to influence these properties, namely, the prehydrolysis conditions, refluxing time, and the use of surfactant. In addition, in some of the preparations under basic conditions $VOCl_3$ was used as vanadia precursor.

The samples prepared under basic hydrolysis had smaller surface areas than those synthesized under acidic hydrolysis. This effect is more evident for the samples prepared following procedure A (Table 1, A10–A12). The adsorption–desorption isotherms for these samples correspond to macroporous-like materials and the pore-size distribution indicates a broad dispersion of the diameter values. However, a comparison of samples A10 and A12 points to the influence of the surfactant's presence that appears to lead to higher surface areas and smaller pores.

The refluxing time has a more marked influence on the textural characteristics than that determined under acidic conditions. The increase of the refluxing time leads to an important decrease of the surface area (Table 1, see A10 and A11). Therefore, following route A, high surface areas were obtained only for small refluxing times.

Preparation under basic hydrolysis was also found to be very sensitive to the nature of the vanadium precursor. However, the relation is not very simple. Replacing VAA with $VOCl_3$ (sample B16 vs B19, and B17 vs B18) led, as a function of the presence of the surfactant, either to an increase or to a decrease in the surface area.

*3.1.3. Influence of prehydrolysis*

Data presented in Table 1 also show differences between the textural properties of the vanadia–silica samples prepared following the different three procedures. Actually, the main difference between these three preparations consist in the way in which the hydrolysis of the two components was carried out: simultaneously (procedure A), previous hydrolysis of silica (procedure B), or previous hydrolysis of both species (procedure C). Depending on the preparation parameters (hydrolysis pH, refluxing time, nature of the vanadia precursor, presence of surfactant) the preparation could be directed to obtain larger surface areas and pores. However, in the case of procedure C, the effect of the surfactant becomes very small (Table 1).

*3.1.4. Influence of the thermal conditions*

The data presented in Table 1 show that the thermal conditions for carrying out the aging of the gels is another important parameter controlling the texture of these materials. Room temperature aging of the gels leads to much higher surface areas compared to the samples prepared under hydrothermal treatment (Table 1, see A1 vs A8, A3 vs A9, B17 vs B19, and C21 vs C22). The pore size is also affected by the thermal treatment of the gels. The samples aged at room temperature exhibit larger pore sizes than those hydrothermally treated.

*3.1.5. Influence of $Cs_2SO_4$ deposition*

Impregnation with $Cs_2SO_4$, followed by calcination at 773 K and cooling at room temperature, leads to thorough changes of the textural characteristics. The surface areas drop dramatically and changes occur also in the pore size and in the pore-size distribution. Most of the samples exhibited pore sizes in the mesoporous range and the pore-size distribution was multimodal.

After $Cs_2SO_4$ deposition the measured surface areas are very small compared to those of the parent materials, and the measurements were not reproducible. Impregnation of the same vanadia–silica support with the same amount of cesium sulfate led to different values of the surface area and pore diameter. The amount of deposited cesium corresponded to a Cs:V molar ratio of 3:1, which does not justify the observed loss of porosity. However, it is known that upon addition of sulfate and heating at 773 K, a reaction occurs between $V_xO_y$ and $Cs_2SO_4$ leading to the formation of a *molten salt* mixture [44], which is distributed in the pores of the carrier and this is demonstrated below by in situ Raman spectra and comparison with Raman spectra of unsupported molten salts. Cooling of the catalyst results in a partial crystallization of the molten salt and formation of glasses which block the mesoporous pores. Therefore the deterioration of the textural properties due to the formation of vanadium–cesium complexes is only an apparent phenomenon. At temperatures where $SO_2$ oxidation occurs, namely at 673–723 K, these complexes exist in a molten state [15], well dispersed on the high surface area mesoporous support.

In summary, procedure A is very sensitive to the preparation parameters (refluxing time, pH, gellification conditions). For example, the increase of the refluxing time in the preparation of samples under basic hydrolysis (A10–

A12) leads to an important decrease of the surface area. On the contrary, for samples obtained under acidic hydrolysis, increasing the refluxing time results in an increase of the surface area. Also, the prehydrolysis of TEOS, and even more of both TEOS and V precursor, made the textural characteristics of the catalysts less sensitive to the preparation parameters. Under these conditions, the materials obtained under basic hydrolysis are still macroporous but the surface areas are much higher and the size of the pores is reduced compared to samples prepared via route A (Table 1, see samples B and C compared to A).

### 3.2. XRD

XRD patterns of vanadia–silica catalysts at temperatures 300–823 K indicate an amorphous structure irrespective of the reaction conditions under which these were prepared. Vanadium is silent in the obtained diagrams, indicating a high dispersion of vanadia. However, as discussed below, $V_2O_5$ crystallites could be observed by means of in situ Raman spectra of $V_2O_5/SiO_2$ catalysts with high surface densities. After deposition of cesium sulfate and following calcination, the only crystalline species observed is $Cs_2SO_4$.

### 3.3. XPS

Table 2 compiles binding energies of the $V_2p_3$ component and the XPS surface distribution, as calculated from V/Si and V/Cs ratios. For vanadia–silica catalysts, except for A11, B15, and B16, which show slightly more oxidized species, vanadium seems to exist in a rather uniform distribution of the oxidation states which corresponds to a $V^{5+}$ state [45,46]. For the same catalysts, the XPS V/Si ratios varied in the range $1.1–4.5 \times 10^{-2}$ showing that the change of the parameters in the sol–gel routes used leads to a different packing of vanadium. These values should be compared to that determined from ICP-AES, namely $8.2 \times 10^{-2}$ which, to a good approximation, was the same for all catalysts.

The deposition of cesium leads to a reduction of the oxidation state of vanadium independent of the way of catalyst preparation (Table 2). The shifts of the binding energies of the $V_{2p3}$ component support this finding. It is worth noting that this is not accompanied by any change in the oxidation state of Cs, the binding energies of which remained essentially the same, namely about 725.2 eV for $Cs_{3d5}$ and 739.2 eV for $Cs_{3d3}$. The changes in the oxidation state are accomplished or may be caused by changes in the surface distribution of vanadium. The data of Table 2 show that the deposition of cesium causes vanadium enrichment on the surface. As observed from the values of the XPS V/Si ratios this enrichment depends on the properties of the impregnated catalyst. In few cases it exceeds the value determined by ICP-AES.

Table 2
XPS binding energies and V/Si and V/Cs ratios for the investigated samples

| Sample | Binding energy of V2p3, eV | | XPS V/Si ratio $\times 10^2$ | | XPS V/Cs ratio |
|---|---|---|---|---|---|
| | $V–SiO_2$ | $V–Cs–SiO_2$ | $V–SiO_2$ | $V–Cs–SiO_2$ | |
| A1 | 518.02 | 517.19 | 3.52 | 10.53 | 0.41 |
| A2 | 518.12 | 517.07 | 2.55 | 6.31 | 0.18 |
| A3 | 518.29 | 517.35 | 2.60 | 10.31 | 0.32 |
| A4 | 518.06 | 517.22 | 2.37 | 5.11 | 0.28 |
| A5 | 518.32 | 516.90 | 4.32 | 13.84 | 0.17 |
| A6 | 518.06 | 517.16 | 1.91 | 7.21 | 0.32 |
| A7 | 518.09 | 517.11 | 4.10 | 4.99 | 0.19 |
| A8 | 517.97 | 517.06 | 1.99 | 5.11 | 0.30 |
| A9 | 517.99 | 517.01 | 2.22 | 4.78 | 0.29 |
| A10 | 518.11 | 517.38 | 2.75 | 3.56 | 0.29 |
| A11 | 518.93 | 517.62 | 2.55 | 4.47 | 0.39 |
| A12 | 518.07 | 517.65 | 2.31 | 7.05 | 0.15 |
| B13 | 518.05 | 517.23 | 1.91 | 3.99 | 0.27 |
| B14 | 518.33 | 517.25 | 3.10 | 7.39 | 0.17 |
| B15 | 518.49 | 516.19 | 1.03 | 2.47 | 0.15 |
| B16 | 518.50 | 517.40 | 1.97 | 4.16 | 0.28 |
| B17 | 518.07 | 517.17 | 1.11 | 2.17 | 0.30 |
| B18 | 518.05 | 517.28 | 4.48 | 5.28 | 0.30 |
| B19 | 518.05 | 517.27 | 2.71 | 4.79 | 0.21 |
| C20 | 517.68 | 516.86 | 1.86 | 4.87 | 0.24 |
| C21 | 517.88 | 516.87 | 2.39 | 5.36 | 0.19 |
| C22 | 517.91 | 516.94 | 2.98 | 5.12 | 0.23 |
| C23 | 517.95 | 517.03 | 3.08 | 7.35 | 0.22 |

### 3.4. Catalytic activity

The catalytic activity will be discussed in relation to the preparation procedure. Nonpromoted catalysts (i.e., without Cs) were found to be inactive with respect to $SO_2$ oxidation. This is in agreement with Dunn et al. [47], who reported TOF values for such catalysts in the order of $10^{-6}$ $s^{-1}$ and attributed this behavior to their structural characteristics [48].

Promoting the $V_2O_5/SiO_2$ catalysts with $Cs_2SO_4$ at a Cs:V ratio of 3 led to a dramatic improvement in the catalytic performance with maximum conversions reached for temperatures in the range 723–773 K. The positive effect of alkali metal sulfates as promoters of vanadia catalysts for $SO_2$ oxidation has been demonstrated long ago [20]. Furthermore, increasing the atomic number of the alkali metal has a beneficial effect in the promotion of the catalyst [18]. In particular, when using Cs as a promoter, it has been shown based on kinetic data that the optimal Cs:V ratio is 3–3.5 [49,50]. The present work demonstrates that after promotion, the samples behaved indeed as usual alkali-promoted supported molten salt catalysts. The performance depended on the procedures by which the vanadia–silica "parent" materials were prepared with a good correlation between the measured surface area and the TOF values.

#### 3.4.1. Activity of samples produced by procedure A

Fig. 1 shows the variation of TOF values (found in the range $1.58–5.65 \times 10^{-3}$ $s^{-1}$) for catalysts prepared by procedure A. The maximum conversions (in the range 70–80%)

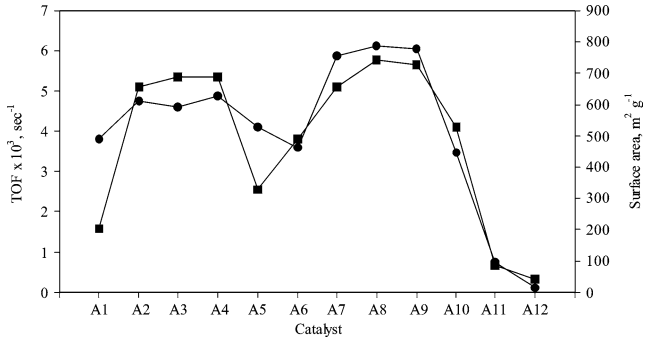


Fig. 1. Variation of the maximum TOF and surface area for the catalysts prepared by procedure A. (■) TOF, (●) surface area.

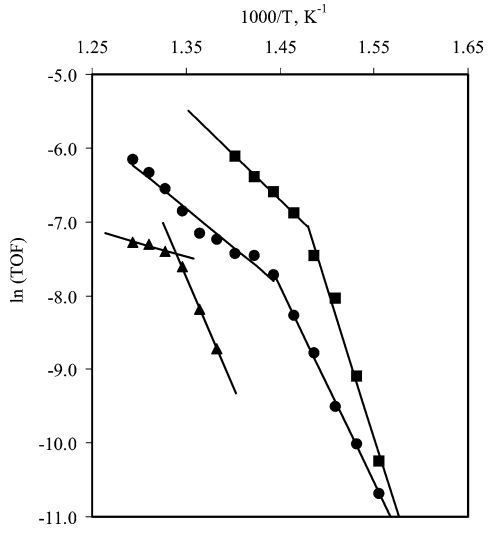


Fig. 2. Arrhenius plots of TOF vs $1/T$ for the catalysts A4Cs (■), A10Cs (●), and A11Cs (▲). 2% $SO_2$, 19% $O_2$, 79% $N_2$, 30 mg catalyst; total flow rate, 100 ml $min^{-1}$.

were found for A2Cs–A4Cs and A7Cs–A9Cs. None of the samples prepared under basic hydrolysis exhibited high activity. A good correlation of the conversion with the surface area was observed, indicating that a higher dispersion of vanadium has a positive effect.

The influence of the refluxing time is directly dependent on the pH at which the hydrolysis is carried out. Longer refluxing times had a positive influence for the materials prepared under acidic hydrolysis. On the contrary, for the samples prepared under basic hydrolysis shorter refluxing times were found to be beneficial. Except for A10 (prepared under short refluxing time), the deposition of Cs on vanadia–silica supports made by basic hydrolysis led to low catalytic performances. The method of the gellification (room temperature or autoclave synthesis) and the nature of the template also influenced the characteristics of the supports. Room temperature reflux in combination with templates like $(CH_3)_3C_{14}H_{29}N$ Br appeared to provide better catalysts.

Fig. 2 shows Arrhenius plots of apparent reaction rates for catalysts A4Cs, A10Cs, and A11Cs. The data correspond to two slope ranges crossing each other in a break point at 675, 694, and 746 K, respectively. Such a dependence was

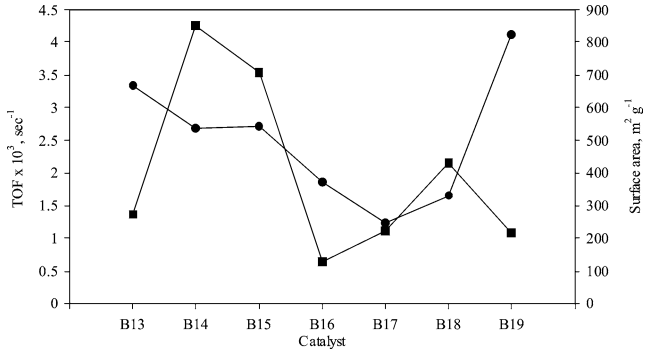


Fig. 3. Variation of the maximum TOF and surface area for the catalysts prepared by procedure B. (■) TOF, (●) surface area.

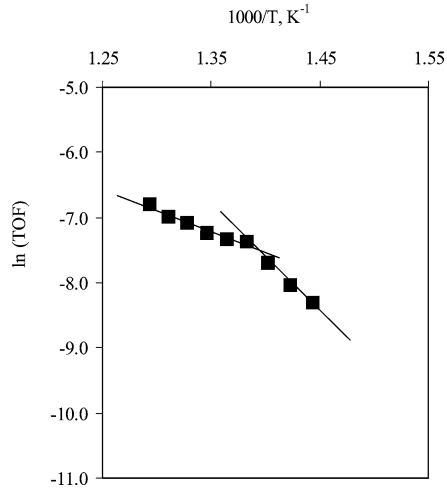


Fig. 4. Arrhenius plot of TOF vs $1/T$ for catalyst B17Cs. 2% $SO_2$, 19% $O_2$, 79% $N_2$, 30 mg catalyst; the total flow rate, 100 ml $min^{-1}$.

found for all the catalysts in this series. The differences occurred in the temperature of the break point ($T_b$). The $T_b$ for A11Cs was 746 K (Fig. 2), i.e., about 70 K higher than in the case of A4Cs. The $T_b$ seems to be strongly related to the catalyst activity, i.e., the higher the activity the lower the $T_b$. This is not surprising in view of the fact that at high conversions (i.e., high $SO_3/SO_2$ ratio) the degree of vanadium reduction ($[V^{4+}]/[V^{5+}]$ is low. Therefore the accumulation of catalytically inactive $V^{4+}$ complexes occurs at lower temperatures [19,51].

### 3.4.2. Activity of samples produced by procedure B

Fig. 3 shows the TOF values for the catalysts prepared by procedure B. The maximum values were determined for B14Cs and B15Cs, which were prepared under acidic hydrolysis using VAA and $VOCl_3$, respectively, as vanadia precursor. Contrary to the catalysts prepared via procedure A, in this case the maximum activity did not coincide with the maximum in the surface area. The highest surface areas were obtained for the catalysts prepared using $VOCl_3$ as vanadia precursor (B13Cs and B19Cs). The TOF values in Fig. 3 correspond to $SO_2$ conversions lower than 60%, i.e., smaller than those exhibited by the catalysts prepared via procedure A. Fig. 4 shows the Arrhenius plot for catalyst

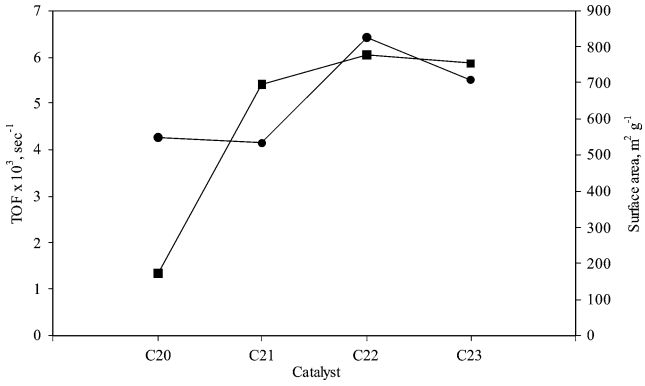


Fig. 5. Variation of the maximum TOF and surface area for the catalysts prepared by procedure C. (■) TOF, (●) surface area.

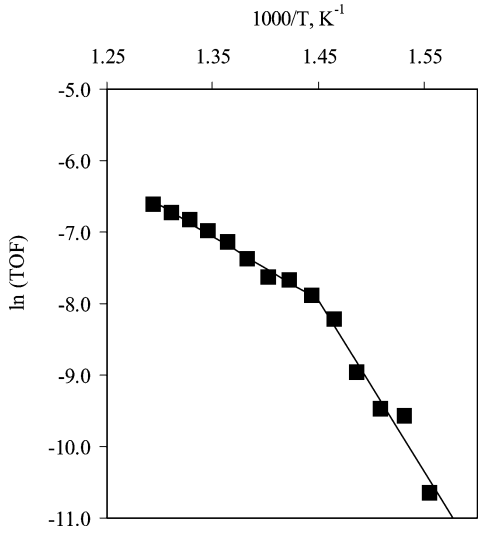


Fig. 6. Arrhenius plot of TOF vs $1/T$ for the catalyst C20Cs. 2% $SO_2$, 19% $O_2$, 79% $N_2$, 30 mg catalyst; total flow rate, 100 ml $min^{-1}$.

B17Cs. The break point ($T_b$) for catalysts prepared using procedure B is found in a narrow temperature range (713–723 K).

### 3.4.3. *Activity of samples prepared by procedure C*

Fig. 5 shows the TOF values for the catalysts prepared via procedure C. Except for C20Cs (prepared using $VOCl_3$ as V precursor) all samples exhibit a good activity. The TOF values shown (around $5 \times 10^{-3}$ $s^{-1}$) correspond to $SO_2$ conversions near 80%. A good correlation between TOF and surface area is found, indicating that also in this case a higher dispersion of vanadium induces a positive effect. Fig. 6 gives the Arrhenius plot for the C20Cs catalyst. In accordance with data determined for other relatively active catalysts, $T_b$ is relatively low, namely 693 K.

Fig. 7 shows the variation of the activation energy for the investigated catalysts, determined from the slope of the ln(TOF) vs $1/T$ plots for the two range of temperatures (see Figs. 2, 4, and 6). In the high-temperature range, where the catalysts were active, the activation energies were smaller than 30 kcal/mol. Except for C21Cs–23Cs, catalysts with

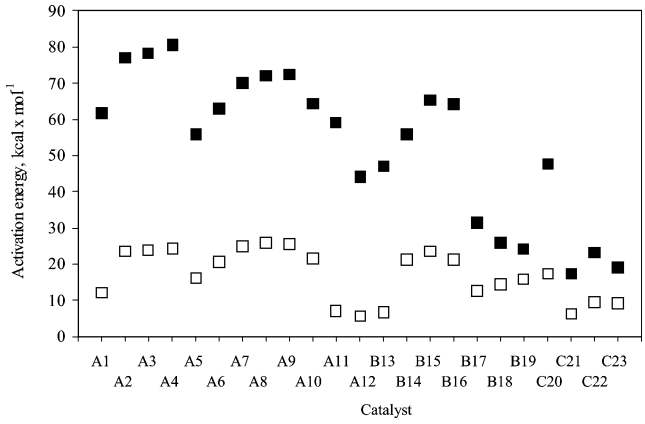


Fig. 7. Variation of the activation energy of the investigated catalysts. (■) Derivation from the low-temperature region; (□) derivation from the high-temperature region.

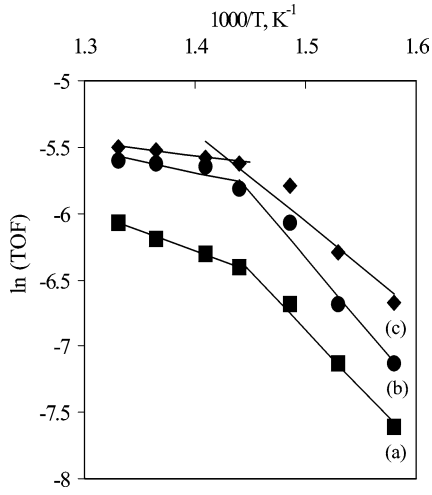


Fig. 8. Arrhenius plots for C21Cs under different conditions. (a) Dry catalyst; (b) treated with 10% $H_2O$; (c) prehydrated.

small activation energies, i.e., smaller than 20 kcal/mol, exhibited low activity (A5Cs, A11Cs–A12Cs, B13Cs, B17Cs–19Cs, seen Figs. 1, 5, and 7). Activation energy smaller than 20 kcal/mol may be indicative of important mass-transfer limitations.

### 3.4.4. *Effect of $H_2O$*

The effect of $H_2O$ was investigated by including 10 vol% $H_2O$ in the feed gas or by prehydration of the catalyst. Fig. 8 shows the ln(TOF) vs $1/T$ for C21Cs under both experimental conditions, and the plot for the dry catalyst is included for comparison. Addition of $H_2O$ led to an increase in the low temperature activity. The effect of $H_2O$ was similar in both cases (i.e., prehydrated catalyst and catalyst treated with 10% $H_2O$), but it had a somewhat different magnitude. However, the initial activity of the catalyst is restored upon changing the feed to dry gas after 4 h.

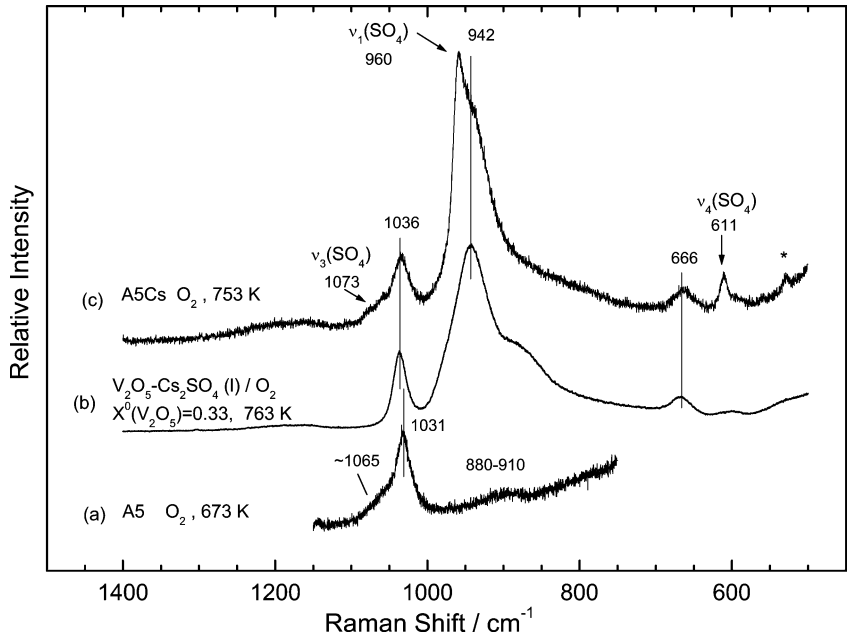


Fig. 9. (a),(c) In situ Raman spectra of $V_2O_5/SiO_2$ A5 catalyst and $V_2O_5$–$Cs_2SO_4/SiO_2$ A5Cs catalyst at $O_2$ atmosphere and temperatures listed by each spectrum; (b) Raman spectrum of the $V_2O_5$–$Cs_2SO_4$ molten mixture with $X^0_{V_2O_5} = 0.33$, obtained under $O_2$.

### *3.5. In situ Raman spectroscopy*

Fig. 9a shows the in situ Raman spectrum of sample A5 under flowing $O_2$. Spectrum c is obtained for sample A5Cs, i.e., after deposition of $Cs_2SO_4$. The samples were exposed to flowing $O_2$ for more than 2 h before recording the spectra, at either 673 or 753 K, as it is labeled in the figure. By comparing spectra 9a and 9c, one can see the difference in the spectral characteristics resulting from the deposition of $Cs_2SO_4$.

The Raman spectrum of the sample prior to Cs deposition (shown in Fig. 9a) is typical for a solid-state $V_2O_5/SiO_2$ catalyst [52] exhibiting an intense peak at 1031 $cm^{-1}$. A well-defined sharp band near 1030 $cm^{-1}$ may evidence the presence of both isolated and surface polymeric species [53,54]. However, there is unanimous agreement among researchers that the surface vanadia species on silica consist of isolated mono-oxo vanadates [55]. Thus the 1031 $cm^{-1}$ band in Fig. 9a is due to V=O terminal bond vibration of isolated, distorted tetrahedral vanadyl species, possessing one V–O bond and three bridging V–O–Si bonds in a $O{=}V{-}(O{-}Si)_3$ configuration. When the monolayer surface coverage is exceeded, crystalline $V_2O_5$ is formed on the catalyst surface [56,57]. Two weaker bands are also seen in Fig. 9a, a shoulder at $\sim$ 1065 and a broad band at 880–910 $cm^{-1}$. These bands are characteristic of Si–O functionalities attributed to perturbed silica vibrations, which are indicative of V–O–Si bonds' formation [52,57].

Raman spectra collected prior to Cs deposition from the various catalytic samples show that the structures of the surface species appear similar among the nonpromoted samples. Small alterations in the relative amounts of the different surface species are attributed to the changes of the surface areas. For example, there is no evidence of crystalline $V_2O_5$ formation in A5 and A9 (with surface densities of 1.44 and 0.96 V atoms/$nm^2$, which are higher than the most commonly reported 0.7 V atoms/$nm^2$ monolayer capacity of the silica carrier [55]). However, it has been noted that certain preparation methods can enhance the surface coverage of the vanadia species on silica up to 2–3 V atoms/$nm^2$ [55]. Therefore, a fairly good dispersion of vanadium must prevail as a result of the sol–gel procedure A, which apparently provides a stronger interaction of vanadia with silica. On the contrary, the in situ Raman spectrum of sample B16 with surface density of 2.04 V atoms/$nm^2$ (obtained under flowing $O_2$ at 753 K, not shown for brevity) exhibits the characteristic 994 $cm^{-1}$ band due to crystalline $V_2O_5$.

After Cs impregnation and calcination, the resulting Raman spectrum of the same catalyst is shown in Fig. 9c. It is known [44], that at 723 K $V_2O_5$ reacts with $Cs_2SO_4$ in the presence of oxygen and the reaction leads to a molten salt that in this case is dispersed on the surface of the silica carrier. Furthermore, a 2:1 $M_2SO_4$:$V_2O_5$ ($M$ = K, Cs) mixture ($X^0_{V_2O_5} = 0.33$) is molten below 723 K and contains $VO_2(SO_4)_2^{3-}$ and $VO_3^-$ units (formed according to $V_2O_5 + 2SO_4^{2-} \rightarrow VO_2(SO_4)_2^{3-} + VO_3^-$) in chain-like and network-like configurations [44]. The Raman spectrum of the *unsupported* $V_2O_5$–$Cs_2SO_4$ molten mixture with $X^0_{V_2O_5} = 0.33$, obtained in $O_2$ atmosphere, is included in Fig. 9b for comparison. Further addition of sulfate (i.e., for $X^0_{V_2O_5} < 0.33$ or Cs:V > 2) results in precipitation of crystalline $M_2SO_4$ [44]. This is exactly the case for the A5Cs investigated catalyst, for which the Cs:V ratio is 3:1 and crystalline $Cs_2SO_4$ is expected to be formed. Indeed, the Ra-

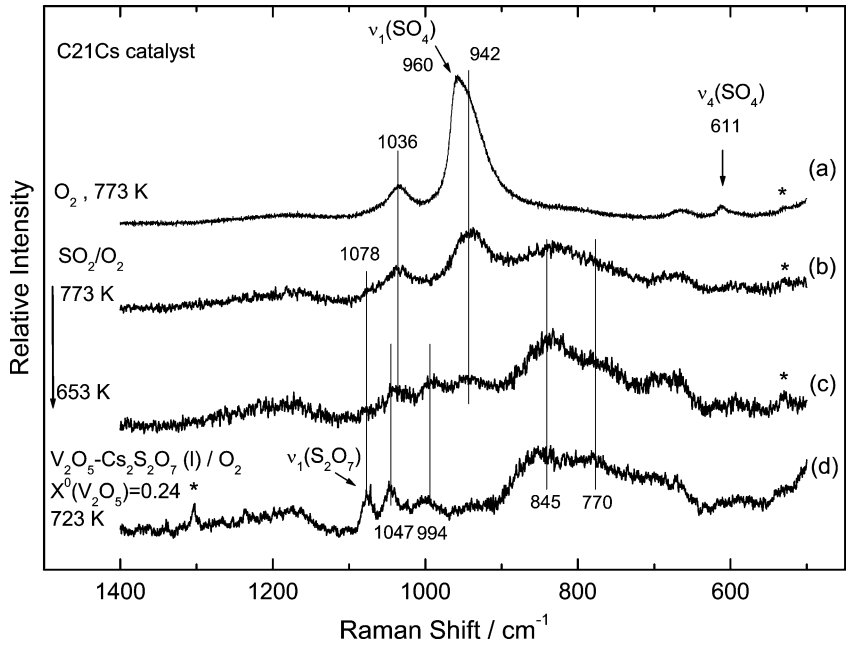


Fig. 10. (a–c) In situ sequential Raman spectra of the C21Cs catalyst at $O_2$ atmosphere, $T = 753$ K (a); at $SO_2/O_2$ atmosphere, $T = 773$ K (b); and at $SO_2/O_2$ atmosphere, $T = 653$ K (c). (d) Raman spectrum of the $V_2O_5$–$Cs_2S_2O_7$ molten mixture with $X^0_{V_2O_5} = 0.24$, obtained under $O_2$.

man spectrum in Fig. 9c consists of superposition of bands due to the molten salt mixture (main bands at 1036, 942, and 667 $cm^{-1}$, which are known [44] to originate from the $V^V$ molten complex $VO_2(SO_4)_2^{3-}$ and $VO_3^-$ units) and bands due to the characteristic $\nu_1$, $\nu_3$, and $\nu_4$ modes of crystalline $Cs_2SO_4$ (at 960, 1073, and 611 $cm^{-1}$).

Fig. 10 shows the in situ sequential Raman spectra of another Cs-promoted catalyst (C21Cs) under a reaction $SO_2/O_2/N_2$ mixture, obtained at 773 K (spectrum b) and 653 K (spectrum c). The spectrum obtained for the freshly calcined sample under $O_2$ at 773 K is included for comparison (Fig. 10a). The 10-fold excess of $O_2$ is sufficient for the conversion of $SO_2$ to $SO_3$, which then reacts with the crystalline $Cs_2SO_4$ forming molten pyrosulfate according to: $SO_4^{2-} + SO_3 \rightarrow S_2O_7^{2-}$. Thus, as seen in Fig. 10b the $\nu_1$, $\nu_3$, and $\nu_4$ sulfate modes of crystalline $Cs_2SO_4$ *disappear*. Furthermore a weak band at 1078 $cm^{-1}$ due to the $\nu_1(S_2O_7^{2-})$ mode appears, indicating a slight excess of molten pyrosulfate. Moreover, $SO_3$ and $S_2O_7^{2-}$ react with the $V^V$ oxosulfato complexes and/or the residual vanadium(V) oxides found at the catalyst surface according to [14,16]:

$$V_2O_5 + 2S_2O_7^{2-} \rightarrow (V^VO)_2O(SO_4)_4^{4-},$$
$$2V^VO_2(SO_4)_2^{3-} + 2SO_3 \rightarrow (V^VO)_2O(SO_4)_4^{4-} + S_2O_7^{2-}.$$

The spectrum of the $(V^VO)_2O(SO_4)_4^{4-}$ molten complex, formed in $V_2O_5$–$Cs_2S_2O_7$ molten mixtures, is known and in order to facilitate the comparison, the spectrum of the $V_2O_5$–$Cs_2S_2O_7$ molten mixture with $X^0_{V_2O_5} = 0.24$ is included in Fig. 10d. Indeed the characteristic 770/845 $cm^{-1}$ strong and broad feature due to the molten dimeric $(V^VO)_2O(SO_4)_4^{4-}$ [14,16,17] appears in spectrum 10b, which consists of superposition of bands due to $V^VO_2(SO_4)_2^{3-}$ (characteristic bands at 1036 and 942 $cm^{-1}$) and $(V^VO)_2O(SO_4)_4^{4-}$ (characteristic bands at 1047, 994, and 845/770 $cm^{-1}$). With decreasing temperature, increasing amounts of the binuclear $(V^VO)_2O(SO_4)_4^{4-}$ species are formed, at the expense of the mononuclear $V^VO_2(SO_4)_2^{3-}$ complex. Significantly, the dinuclear $(V^VO)_2O(SO_4)_4^{4-}$ molten complex has been identified as the active species in the catalytic cycle of $SO_2$ oxidation in $V_2O_5$-based supported molten salt catalysts [15,17]. The lower signal-to-noise ratio in spectra 10c and 10d is due to the much darker (dark brown) color of the $V_2O_5$–$Cs_2S_2O_7$ melts relative to the color of $V_2O_5$–$Cs_2SO_4$ melts in oxygen atmosphere [16].

### 3.6. In situ EPR spectra

Comparative in situ EPR spectra during activation of the catalysts under dry and wet conditions (10% $H_2O$) indicated the influence of $H_2O$ on the degree of polymerization on the part of vanadium present as $VO^{2+}$ in the Cs-promoted C21Cs catalyst (Figs. 11a and b). During dry calcination relatively well-defined axial symmetric, immobilized, but isolated $VO^{2+}$ units are present at 373 K, and their relative amount increases significantly at 473 K. At 573 K a loss of symmetry of these species is observed due to splitting of the perpendicular features of the characteristic axial $VO^{2+}$ spectrum. This is most clearly seen at $g$ values around 1.85. This indicates that structural changes occur in the catalyst, probably due to $H_2O$ ligands evaporating. At 673 K the hyperfine features of the observed spectrum regain symmetry, most probably because the vanadium species have been dissolved in a molten salt solvent. This introduces the so-called

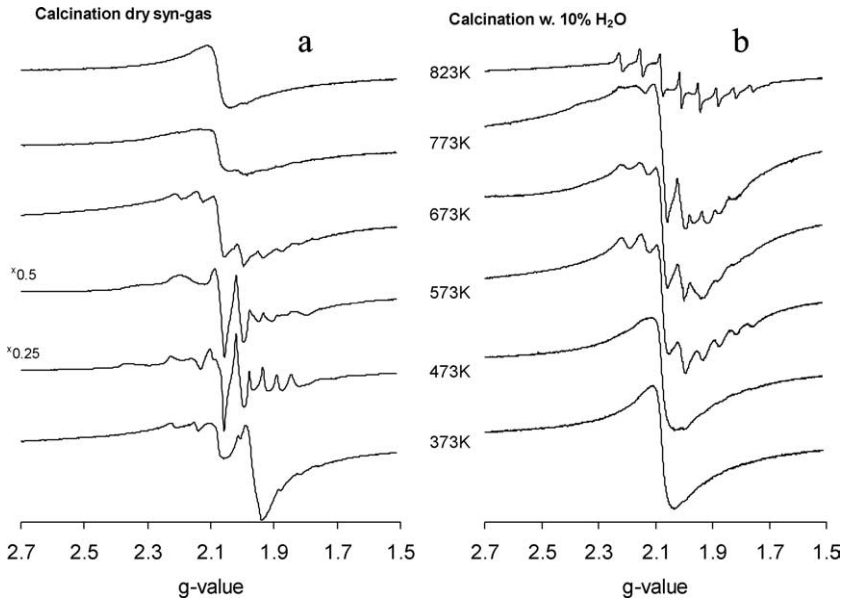


Fig. 11. Comparative in situ EPR spectra during activation of the catalysts under dry (a) and wet conditions (b) for the cesium-promoted C21Cs catalyst.

tumbling effect, where the observed $VO^{2+}$ signal is an average of the contributions from the three primary ($g_x$, $g_y$, $g_z$) tensors. At 773–823 K the signal of these isolated $VO^{2+}$ decreased and a broad band of remaining polymeric vanadium species is observed.

During the wet calcination very little solid state-immobilized $VO^{2+}$ is seen at 373–473 K, but a broad band probably from polymeric vanadium species dominates. However, it is clear that a molten salt solvent is present already at 573 K, since a significant hyperfine structure from isolated, but dissolved, $VO^{2+}$ units is observed. This was not seen until 673 K in the dry calcination procedure, but it is reasonable from a physicochemical point of view for the wet system, since $H_2O$ acts as a freezing point depresser. However, at 673 and 773 K it appears that $H_2O$ evaporates, i.e., the system is again in solid state and axial symmetric $VO^{2+}$ units are observed. At 823 K the vanadium–sulfate system melts completely, and a well-defined spectrum of monomeric $VO^{2+}$ complexes in solution is observed. As compared to the 823 K spectrum of the dry calcined catalyst, there is a very clear effect of $H_2O$ in the sense that it reacts with the melt and breaks up polymeric V(IV) species, leaving an amount of more mobile paramagnetic complexes in the melt.

Fig. 12 shows the *operando* EPR spectra obtained simultaneously with activity measurements at steady state, where the catalyst is sequentially cooled from 823 to 613 K. According to the activity data (shown in Fig. 8), a marked break point, indicative of phase changes, occurs at 693–703 K. However, as seen from the EPR spectra, crystallization of V(IV) compounds does not occur until 613 K, where a sharp peak with $g = 1.970$ appears in the EPR spectrum. This is probably due to formation of the compound $Cs_2(VO)_2(SO_4)_3$ [18,19]. In the temperature region 703–753 K a rather steady decreasing amount of monomeric

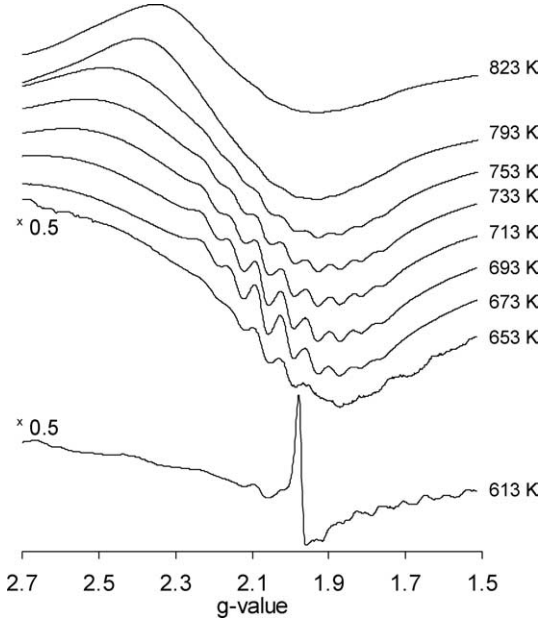


Fig. 12. EPR spectra obtained simultaneously with series of activity measurements at steady state, where the C21Cs catalyst is sequentially cooled down from 823 to 613 K.

$VO^{2+}$ complexes is observed. The deactivation of the catalyst in the noted temperature range must therefore be due to crystallization of EPR silent $V^{3+}$ or $V^{5+}$ compounds. This behavior and the difference between $T_b$ (temperature of the break point in the Arrhenius plot) and $T_p$ (temperature of precipitation as observed in the operando EPR spectra) have been addressed before [58]. At 613 K and below, both $V^{4+}$ and probably also $V^{5+}$ crystalline compounds are found in the catalyst as deactivated vanadium compounds.

### 3.7. Structure-activity relationships and catalytic performance

The formation of molten vanadium oxosulfato complexes in Cs-promoted vanadia catalysts is crucial for the catalytic performance and the structural properties of the active melt have been thoroughly characterized [11–18] and the results of this study suggest that the catalytic activity is related to the formation of the same molten vanadium oxosulfato complexes. This is well established by comparing the Raman spectra of the Cs-promoted catalysts to unsupported model molten salt/gas systems [14,16,17,44,64].

The relation between the surface area of the support and vanadia loading in molten salt catalysts is well known [59]. It was shown that the surface area of silica containing large pores, generally not exceeding 300 $m^2\,g^{-1}$, did not allow the deposition of $V_2O_5$ loadings higher than 7 wt%. Further increase in the concentration of the components causes thickening of the active molten salt layer, filling of wider pores and additional reduction in the effective surface, thus leading to lower reaction rates. Calculations made by the group of Boreskov [60,61] indicated that the maximum thickness of the active component film at which diffusion retardation does not occur is about 600 Å. Such a high value suggests also the existence of a nonuniform distribution of the active component on the carrier. The same authors indicated that the effective film thickness of the molten salt decreased with decreasing temperature, and increased with increasing conversion [62]. Studies concerning the effect of the pore radius on the activity of V–K catalysts supported on silica gel indicated that a maximum in activity was achieved for a pore radius of 100 Å [61].

Data obtained in this study suggest a correlation between the catalytic activity and surface area but the effect of the pore radius is more complicated. The apparent activation energies at $T > T_b$ (i.e., above the break point, Figs. 2, 4, 6, and 7) pointed in several cases to the existence of mass-transfer limitations (values lower than 20 cal $mol^{-1}$). This was more evident in the case of C21Cs–C23Cs, which also showed a high activity. For some other active catalysts A3Cs–A4Cs or A8Cs–A9Cs, the apparent activation energy at $T > T_b$ had values that may exclude the existence of mass-transfer limitations. However, no clear dependence on the pore size could be observed from the large series of investigated catalysts. Previous studies of unsupported melt systems [18,19] indicated that under such conditions the reaction is controlled by mass-transfer limitations. However, it is remarkable that gases with low content of $SO_2$ could be oxidized with rather high TOF.

Arrhenius plots of the apparent rate constant for the $SO_2$ oxidation over vanadia catalysts invariably show a break at temperatures typically below 723 K, and the activation energy is very high in the low-temperature region [18,19,21,63]. This phenomenon has been connected to the presence of V species of lower oxidation state at low temperatures [63] and was furthermore attributed to formation and precipitation of $V^{4+}$ and $V^{3+}$ crystalline compounds below the temperature of the break point in the Arrhenius plots [18,19]. The presence of water in the gas feed had a positive effect in catalyst activity. Recent studies on vanadia–pyrosulfate-supported liquid-phase catalysts [58] indicated that depending on the support composition the presence of water might have a beneficial effect in catalytic activity. The content of water is also important for the transformation of pyrosulfate into hydrogen sulfate species. These effects are also reflected in the Arrhenius plots of apparent reaction rates vs $1/T$, resulting in different break temperatures and higher apparent activation energies.

## 4. Conclusions

Vanadia–silica catalysts prepared by various sol–gel procedures exhibit high surface areas and well-dispersed vanadium. These preparations are sensitive to the sol–gel parameters. Following these routes of synthesis mesoporous or macroporous vanadia–silica catalysts with a fairly sharp pore-size distribution could be obtained. Further impregnation with cesium sulfate causes dissolution of vanadia in a molten salt, resulting in the formation of vanadium oxosulfato complexes, which at high temperatures are molten and distributed in the mesoporous support. These complexes are effective catalysts for oxidation of $SO_2$ in dilute gases. High surface area of these materials ensures a good dispersion of the melt, leading to satisfactory conversions at high space velocities. The preparation method of the mesoporous vanadia–silica support and the nature of the vanadium precursor give rise to differences in the catalytic behavior.

## Acknowledgments

NATO's Scientific Affairs Division in the framework of the Science for Peace Programme (SfP 971984) has sponsored this research. Support from the General Secretariat of Research and Technology of the Greek Ministry of Development, the Romanian Ministry of Science and Education, and the Danish Technical Research Council is gratefully acknowledged.

## References

[1] J.N. Armor, Appl. Catal. B 1 (1992) 221.
[2] S.N.R. Rao, E. Waddell, M.B. Mitchell, M.G. White, J. Catal. 163 (1996) 176.
[3] D. Uy, A. Dubkov, G.W. Graham, W.H. Weber, Catal. Lett. 68 (2000) 25.
[4] J. De Wilde, G.B. Marin, Catal. Today 62 (2000) 319.
[5] A. Bhattachararyya, G.M. Woltermann, J.S. Yoo, J.A. Karch, W.E. Cormier, Ind. Eng. Chem. Res. 27 (1998) 1356.
[6] J.S. Buchanan, D.L. Stern, K.E. Nariman, G.J. Teitman, J.F. Sodomin, D.L. Johnson, Ind. Eng. Chem. Res. 35 (1992) 2495.
[7] S.M. Duranni, Environ. Sci. Technol. 28 (1994) 88.
[8] S. Blumrich, B. Engler, Catal. Today 17 (1993) 301.

[9] G.K. Boreskov, Sh.Yu. Matros, O.V. Kiselev, G.A. Bunimovich, Dokl. Akad. Nauk USSR 237 (1997) 160.
[10] Yu.Sh. Matros, Catalytic Processes under Unsteady-State Conditions, Elsevier, Amsterdam, 1989.
[11] G.E. Folkmann, G. Hatem, R. Fehrmann, M. Gaune-Escard, N.J. Bjerrum, Inorg. Chem. 30 (1991) 4057.
[12] K. Nielsen, R. Fehrmann, K.M. Eriksen, Inorg. Chem. 32 (1993) 4825.
[13] G.E. Folkmann, K.M. Eriksen, R. Fehrmann, G. Hatem, M. Gaune-Escard, O.B. Lapina, V. Terskikh, J. Phys. Chem. B 102 (1998) 24.
[14] S. Boghosian, F. Borup, A. Chrissanthopoulos, Catal. Lett. 48 (1997) 145.
[15] O.B. Lapina, B.S. Bal'zhinimaev, S. Boghosian, K.M. Eriksen, R. Fehrmann, Catal. Today 51 (1999) 469.
[16] S. Boghosian, A. Chrisanthopoulos, R. Fehrmann, J. Phys. Chem. B 106 (2002) 49.
[17] A. Christodoulakis, S. Boghosian, J. Catal. 215 (2003) 319.
[18] S. Boghosian, R. Fehrmann, N.J. Bjerrum, G.N. Papatheodorou, J. Catal. 119 (1989) 121.
[19] K.M. Eriksen, D.A. Karydis, S. Boghosian, R. Fehrmann, J. Catal. 155 (1995) 32.
[20] H.F.A. Topsøe, A. Nielsen, Trans. Dan. Acad. Technol. Sci. 1 (1947) 18.
[21] F. Doering, D. Berkel, J. Catal. 103 (1987) 126.
[22] I.E. Wachs, R.Y. Saleh, S.S. Chan, C.C. Chersich, Appl. Catal. 15 (1985) 339.
[23] G. Deo, I.E. Wachs, J. Catal. 146 (1994) 323.
[24] G. Deo, I.E. Wachs, J. Catal. 146 (1994) 335.
[25] A.J. Van Hengstrum, J.G. van Ommen, H. Bosch, P.J. Gellings, Appl. Catal. 8 (1983) 368.
[26] H. Knozinger, E. Taglauer, Catalysis 10 (1993) 1.
[27] G. Hausinger, H. Schmelz, H. Knozinger, Appl. Catal. 39 (1988) 267.
[28] J. Haber, T. Machej, E.M. Serwicka, I.E. Wachs, Catal. Lett. 32 (1995) 101.
[29] J. Haber, T. Machej, T. Czeppe, Surf. Sci. 151 (1985) 301.
[30] K. Habersberg, P. Jiru, Z. Tvaruzkova, G. Centi, F. Trifiro, React. Kinet. Catal. Lett. 39 (1989) 95.
[31] J.S. Reddy, A. Sayari, Catal. Lett. 28 (1994) 263.
[32] F. Cavani, F. Trifiro, P. Jiru, K. Habersberg, Z. Tvaruzkova, Zeolites 8 (1988) 12.
[33] J. Haber, A. Kozlowska, R. Kozlowsi, J. Catal. 102 (1986) 52.
[34] M.M. Koranne, J.G. Goodwin, G. Marcelin, J. Catal. 148 (1994) 369.
[35] G.C. Bond, K. Bruckman, Chem. Soc., Faraday Disc. 72 (1981) 235.
[36] M.D. Curran, Th.E. Gedris, A.E. Stiegman, G.A. Plett, Chem. Mater. 11 (1999) 1120.
[37] A. Baiker, Stud. Surf. Sci. Catal. 101A (1996) 51.
[38] D.C.M. Dutoit, M.A. Reiche, A. Baiker, Appl. Catal. B 13 (1997) 275.
[39] R. Rulkens, J.L. Male, K.W. Terry, B. Olthof, A. Khodakov, A.T. Bell, E. Iglesia, T.D. Tilley, Chem. Mater. 11 (1999) 2966.
[40] J. Livage, Catal. Today 41 (1998) 3.
[41] L. Sim, G.L. Haller, Appl. Catal. A 188 (1999) 277.
[42] C. Oehlers, R. Fehrmann, S.G. Masters, K.M. Eriksen, D.E. Sheinin, B.S. Bal'zhinimaev, V.I. Elokhin, Appl. Catal. A 147 (1996) 127.
[43] D.A. Karydis, S. Boghosian, R. Fehrmann, J. Catal. 145 (1994) 312.
[44] S. Boghosian, J. Chem. Soc., Faraday Trans. 94 (1998) 3463.
[45] Ch. Fountzoula, M.K. Matralis, Ch. Papadopoulou, G.A. Voyiatzs, Ch. Kordulis, J. Catal. 184 (1999) 5.
[46] M.K. Matralis, M. Ciardelli, M. Ruwet, P. Grange, J. Catal. 157 (1995) 368.
[47] J.P. Dunn, P.R. Koppula, H.G. Stenger, I.E. Wachs, Appl. Catal. B 19 (1998) 103.
[48] J.P. Dunn, P.R. Koppula, H.G. Stenger, I.E. Wachs, Catal. Today 51 (1999) 301.
[49] F.J. Doering, React. Kinet. Catal. Lett. 39 (1989) 1.
[50] G.K. Boreskov, A.A. Ivanov, B.S. Balzhinimaev, L.M. Karatovskaya, React. Kinet. Catal. Lett. 14 (1968) 25.
[51] D.A. Karydis, K.M. Eriksen, R. Fehrmann, S. Boghosian, J. Chem. Soc., Dalton Trans. (1994) 2151.
[52] S. Xie, E. Iglesia, A.T. Bell, Langmuir 16 (2000) 7162.
[53] M.A. Banares, I.E. Wachs, J. Raman Spectrosc. 33 (2002) 359.
[54] A. Christodoulakis, M. Machli, A.A. Lemonidou, S. Boghosian, J. Catal. 222 (2004) 293.
[55] I.E. Wachs, B.M. Weckhuysen, Appl. Catal. A 157 (1997) 67.
[56] A. Khodakov, B. Olthof, A.T. Bell, E. Inglesia, J. Catal. 181 (1999) 205.
[57] X. Gao, S.R. Bare, B.M. Weckhuysen, I.E. Wachs, J. Phys. Chem. B 102 (1998) 10842.
[58] S.G. Masters, A. Chrissanthopoulos, K.M. Eriksen, S. Boghosian, R. Fehrmann, J. Catal. 166 (1997) 16.
[59] K. Nowinska, Z. Phys. Chem. Neue Folge 126 (1981) 117.
[60] G.M. Polyakova, G.K. Boreskov, A.A. Ivanov, L.P. Davydova, G.A. Marochkina, Kinet. Katal. 12 (1971) 586.
[61] P. Belyaeva, B.S. Balzhinimaev, L.G. Simonova, V.I. Zaikovskii, A.A. Ivanov, G.K. Boreskov, React. Kinet. Catal. Lett. 30 (1986) 9.
[62] B.S. Balzhinimaev, V.E. Ponomarev, G.K. Boreskov, A.A. Ivanov, React. Kinet. Catal. Lett. 25 (1984) 219.
[63] G.K. Boreskov, G.M. Polyakova, A.A. Ivanov, V.M. Mastikhin, Dokl. Akad. Nauk SSSR 210 (1973) 626.
[64] I. Giakoumelou, R.M. Caraba, V. Parvulescu, S. Boghosian, Catal. Lett. 78 (2002) 209.